Evaluation of nanocellulose-based anthraquinone from marine fungi *Penicillium flavidorsum* as an alternative therapy for skin wound healing: histopathological and immunohistochemical evidences from a rat model

Reham Reda[1], Doaa H. Assar[2], Ibrahim I. Al-Hawary[1], Ayman Atiba[3], Alaa Abdelatty[4], Norah Althobaiti[5] and Zizy I. Elbialy[1*]

Abstract

Background Wound healing represents a complex clinical challenge, necessitating the selection of appropriate wound dressings to facilitate an efficient healing process. This study aims to explore an effective approach to enhance wound healing by investigating the therapeutic potential of a nanocellulose-based anthraquinone derived from marine fungi.

Forty male Wistar rats were divided into five groups, including a control group and various four treatment groups. The wound healing process was assessed by measuring the wound area at different time points.

Results The results showed promising outcomes in terms of wound healing progression. The group treated with anthraquinone and nanocellulose demonstrated the most favorable results, with normal epidermal architecture, marked hyperkeratosis, and minimal dermal edema. This study provides comprehensive evidence supporting the efficacy of this novel alternative therapy through histopathological and immunohistochemical analyses conducted on a rat model.

Conclusion By addressing the limitations associated with conventional wound dressings, our research contributes to the development of innovative strategies for optimizing wound healing outcomes. The findings presented herein underscore the potential of nanocellulose-based anthraquinone as a promising therapeutic option for promoting skin wound healing. Further investigations are warranted to elucidate the underlying mechanisms and establish the clinical viability of this alternative therapy.

Keywords Nanocellulose, Anthraquinone, Wound healing, Marine fungi

*Correspondence:
Zizy I. Elbialy
zeze_elsayed@fsh.kfs.edu.eg
Full list of author information is available at the end of the article

Reda *et al. Beni-Suef Univ J Basic Appl Sci*   (2024) 13:63

Page 2 of 11

1 Background

Wound healing involves a sophisticated physiological process that encompasses a series of intricate cellular and molecular mechanisms aimed at restoring damaged tissue integrity [1, 2]. The dynamic process of wound healing involves complex interactions among cells, components of the extracellular matrix, and biochemical signaling pathways [3, 4].

Throughout the years, the progression of wound dressing technology has markedly advanced from the introduction of the first contemporary dressing in the mid-1980s. These dressings were designed to keep a moist environment, help absorb fluids, minimize infection, and promote wound healing and management [5]. Modern wound dressings are now identified as interactive and bioactive remedies, merging the physical barrier offered by conventional dressings with the addition of specific bioactive molecules. These molecules promote cell renewal through the proliferation and migration of fibroblasts and keratinocytes, boost collagen production, fight against bacterial infections, and aid in drug delivery, all of which contribute to an effective healing process. A perfect wound dressing ought to preserve a high level of humidity at the wound location, absorb excess exudate, display non-toxic and hypoallergenic characteristics, permit oxygen transfer, guard against microbial intrusion, and be both comfortable and economical. Modern dressings take various forms, such as hydrogels, foams, sponges, films, and recently, nanofibrous mats [6–8].

There is a growing demand for sustainable, eco-friendly nanoscale materials. Biomass-derived polymers like cellulose are gaining attention due to their abundance, easy extraction, biocompatibility, non-toxicity, and biodegradability. Cellulose, in particular, is being considered for wound dressings, either as an additive or a primary material. Data indicate promising outcomes, especially in terms of cell proliferation and attachment [9, 10].

Employing nanomaterials in wound therapy can address the shortcomings of conventional wound care and enhance the healing process [11]. Consequently, there is a rising need for new treatment approaches to tackle these problems and speed up wound healing. In recent years, nanotechnology has made significant progress and holds great potential for numerous medical applications, including wound healing. [12, 13]. Nanomaterials offer specific advantages that could transform wound treatment because of their unique physicochemical properties and nanoscale dimensions [14]. These materials can modulate biological processes at both the cellular and molecular levels due to their tailored surface properties, high surface-to-volume ratios, and other characteristics. As a result, nanomaterials have garnered significant attention as versatile tools for creating innovative wound healing therapies [15, 16].

Fungi sourced from marine environments have a diverse biosynthetic machinery that allows them to produce a wide range of secondary metabolites from different chemical classes, such as alkaloids, polyketides, terpenoids, meroterpenoids, peptides, and steroids [17–20].

Among the fungal secondary metabolites, anthraquinones, especially 1,8-dihydroxy-anthraquinones, are among the most researched compounds due to their recognized pharmacological properties [21]. Anthraquinones (AQs) belong to a group of phenolic substances distinguished by a 9,10-anthracenedione (also referred to as 9,10-dioxoanthracene) core structure, featuring three fused benzene rings with two ketone groups on the central ring [19, 22]. Remarkably, anthraquinones and their derivatives are gaining more interest due to their diverse biological activities, which include acting as laxatives [23], antifungals [24], antibacterials [25], antimalarials [26], anti-inflammatories [27, 28], antiarthritics [28], diuretics [27], antiplatelets [29, 30], neuroprotectives [31], and having anticancer properties [22, 32–35].

In light of wound healing demands for effective therapies to accelerate tissue regeneration, active biomolecules with healing abilities have been incorporated into nanostructured polymeric dressings. The synergistic effects of these combinations need to be investigated. This study aims to introduce a novel wound healing approach by exploring the therapeutic potential of nanocellulose-based anthraquinone derived from marine fungi, positioning it as a sustainable and effective alternative therapy for skin wound healing in a rat model through comprehensive histopathological and immunohistochemical analyses.

2 Methods

2.1 Experimental animals

Forty 10-week-aged male Wistar rats, weighing 110 ± 10 g, were purchased from a confined Animal House Colony. The rats were kept individually in plastic cages to prevent interferences such as biting and potential wound scratching from other animals. They were provided with a standard diet (Al Wadi Co., Giza, Egypt) [9] and had water *ad libitum*. The animals were kept in a laboratory maintained at a temperature of 25 ± 2 °C. A 1-week acclimatization period was observed before the commencement of the study to allow the animals to adapt to their new environment.

2.2 Ethical approval

Follow the normal operating procedures approved by the Institutional Animal Care and Animal Ethics Committee,

Reda *et al. Beni-Suef Univ J Basic Appl Sci*   (2024) 13:63

Page 3 of 11

Faculty Aquatic and Fisheries Sciences, Kafrelsheikh University, Egypt (IAACUC-KSU-005-2021).

2.3 Experimental design
Following the acclimatization period, excisional skin wounds of 1.5×1.5 cm in diameter were performed on the dorsal region of each rat (Fig. 1A, B). The experimental animals ($n = 40$) were then divided randomly into five experimental groups, with eight rats per group, as follows:

I. Control group (G1): untreated skin wound group.

II. Hydrogel treated group (G2): skin wound group treated with hydrogel only.

III. Anthraquinone treated group (G3): skin wound group treated with anthraquinone.

IV. Anthraquinone and nanocellulose treated group (G4): skin wound group treated with both anthraquinone and nanocellulose.

V. Nanocellulose alone treated group (G5): skin wound group treated with nanocellulose.

The amount used from hydrogel, anthraquinone, nanocellulose to cover the whole wound area.

2.4 Establishment of full thickness dermal excisional wound
To carry out the excisional wounds, the rats were anesthetized with a combination of ketamine and xylazine administered via intraperitoneal injection (ketamine 70 mg/kg and xylazine 7 mg/kg). The back hair of the rats was then shaved, and the area was disinfected using 70% ethanol. Full-thickness skin excisional wounds measuring 1.5×1.5 cm were created on the dorsal region of each animal, following the protocol described by Atiba et al. [36]. The wound areas were measured then photographed using special size analysis software, NIH Image J software (available at http://www.rsb.info.nih.gov/ij), at various time points: 0, 3, 6, 9, 12, 15, 17, and 19 days post-wounding (Fig. 2). The alteration in wound dimensions was measured in terms of a percentage in comparison with the initial wound size (day 0), and the results are
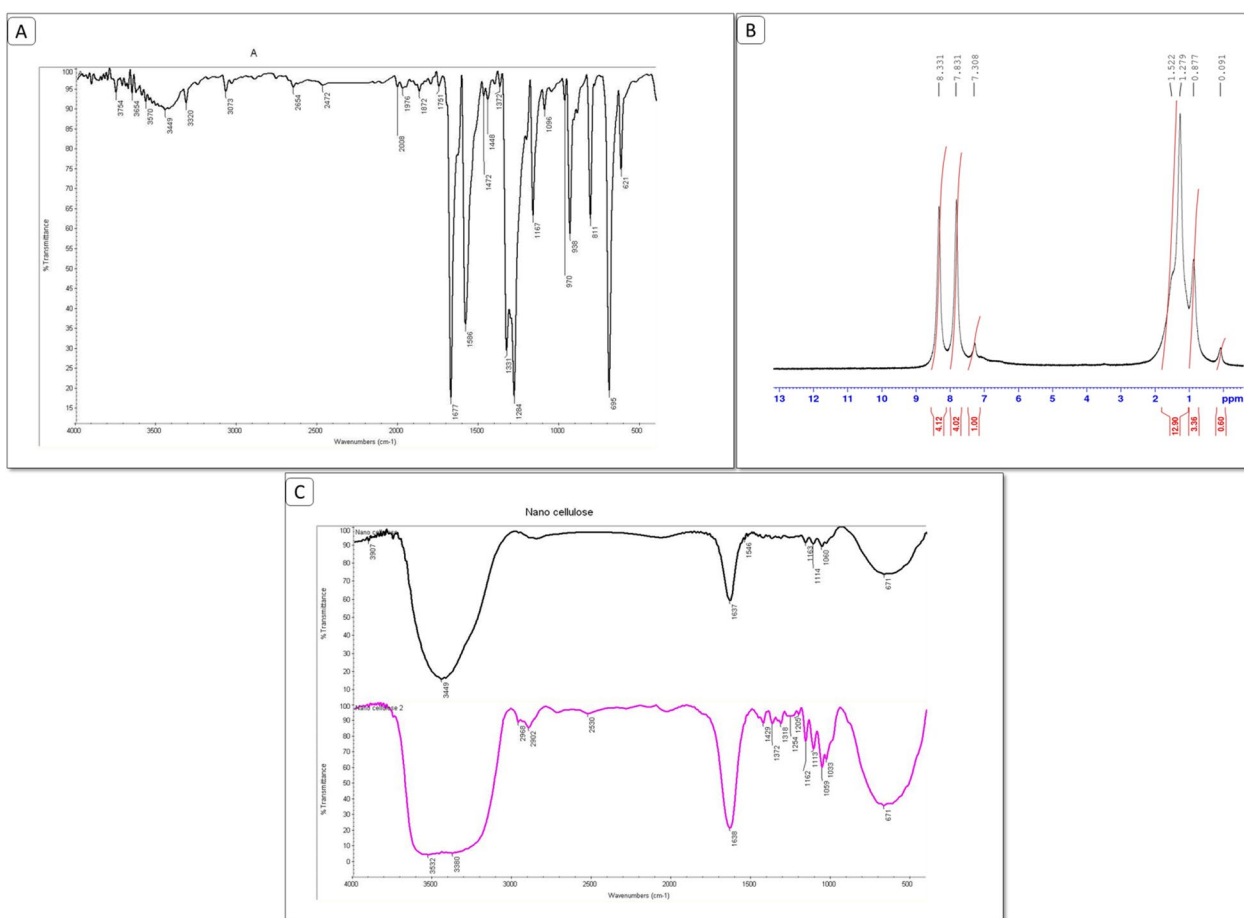
Fig. 1 **A** FTIR spectra of extracted anthraquinone. **B** H NMR data of anthraquinone compound in CDCL3 (400 MHz) obtained from marine fungi. **C** FTIR analysis for nanocellulose

Reda *et al. Beni-Suef Univ J Basic Appl Sci*   (2024) 13:63

Page 4 of 11
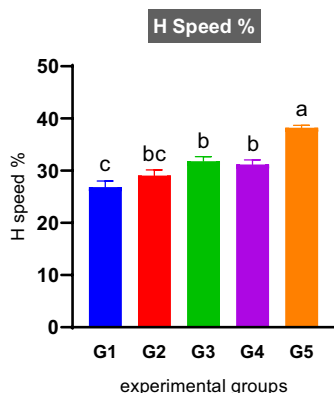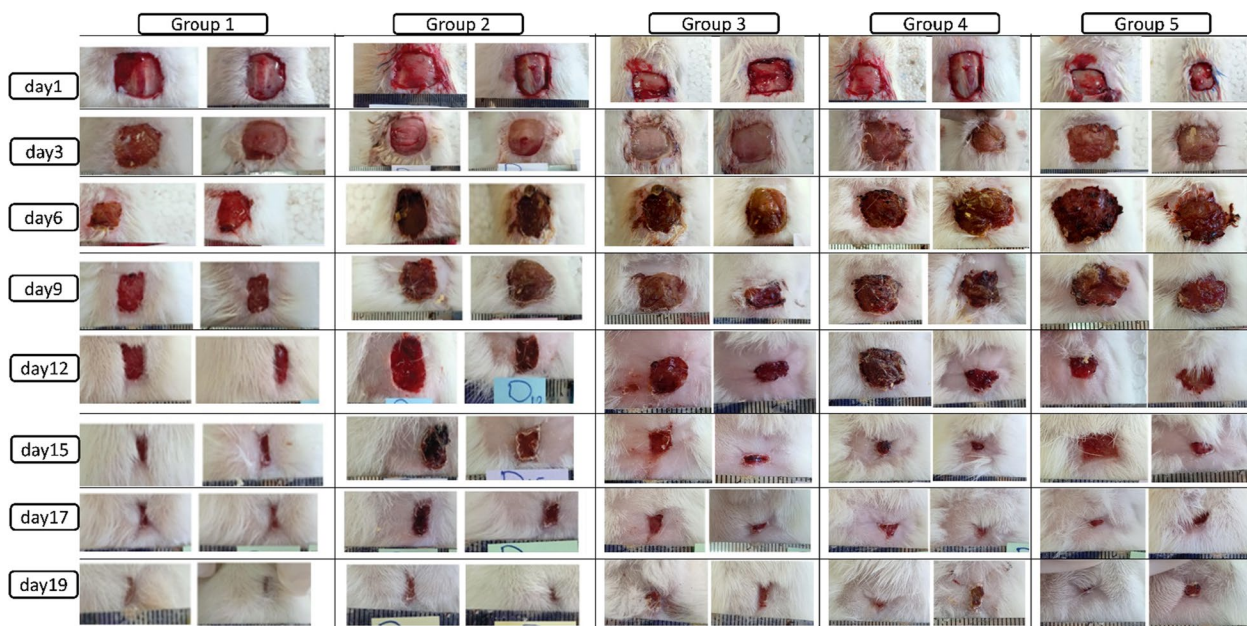
Fig. 2 **A** Wound area measurement. **B** Healing speed measurement

presented in Fig. 2. The medical dressings were changed for the excisional wound groups on the specified days, with careful inspection of the wound healing progress.

2.5 Isolation of bioactive compounds from marine *fungi*

All chemicals, solvents and reagents used were of analytical grade. The chemicals used from Sigma® and Alpha for chemicals and were of the purest grade available.

2.5.1 Sample collection and preparation

2.5.1.1 Fungal material A diverse array of marine fungi and other microorganisms collected from marine water from Alexandria beach at a depth of 3 m. The collected sample (from five different locations) was carefully placed into a clean plastic bag and immediately transported to the laboratory. Upon arrival, the sample was stored at −20 °C to preserve its integrity and ensure its suitability for further analysis. To facilitate fungal growth, a cul-

ture medium was prepared using potato agar following a standardized protocol [37]**.**

2.5.1.2 Extraction of fungal anthraquinone using ethanol The extraction of anthraquinone from the fungal culture was performed using an ethanol-based extraction method [38]**.** The resulting extract, as well as its fractions and sub-fractions, were subjected to monitoring through high-performance liquid chromatography (HPLC) to assess their composition and purity. Additionally, Fourier transform infrared (FTIR) analysis was performed in order to provide further insights into the chemical characteristics and structural properties of the extracted compounds.

The final extract contained 76.2% anthraquinone.

2.5.1.3 Fermentation Culture of fungal strains on slants with PDA at 28 °C for 7 days. Inoculation under static

Reda *et al. Beni-Suef Univ J Basic Appl Sci*   (2024) 13:63

Page 5 of 11

conditions at room temperature in conical flask contains 300-ml Wickerham's medium for fermentation for one month. To stop the fermentation process, 300-ml EtOAc was added to the contents of the flask and centrifuge. Then, the content was filtered using Buchner funnel, and the filtrate was then transferred to separating funnel. Separate the aqueous phase and the EtOAc phase, the aqueous phase is then extracted several times with EtOAc till exhaustion. The combined EtOAc extracts was then evaporated under vacuum to obtain a solid or oily residue. The residue was then suspended in 90%MeOH fractionated with *n*-hexane, and water was added to render the MeOH 60% and then fractionated with ethyl acetate and butanol. Then, the extract was characterized by FTIR and nuclear magnetic resonance (NMR) spectroscopy [39].

2.6 Chemical test for anthraquinones detection

2.6.1 Detection of anthraquinone using Borntrager's test

To confirm the presence of anthraquinone in the extract, Borntrager's test, as described by Harborne et al. [40], was used. By preparing 1 g of anthraquinone, 10 ml of dilute HCl was boiled on water bath for 10 min and then filtered. The filtrate was extracted using benzene, and an equal volume of ammonia solution was added to the filtrate, followed by shaking. The emergence of a pink color in the ammoniacal layer indicates the presence of the anthraquinone moiety.

2.7 FTIR (Fourier transform infrared)

The FTIR analysis method uses infrared light to scan test samples and observe chemical properties (Riaz et al. [41]). The major parameters' settings for FTIR were the 4 cm^{-1} resolution and scan number of 64 times; the transmission spectrum within 450–4000 cm^{-1} was recorded.

2.8 Nanocellulose preparation

Nanocellulose was prepared using acid hydrolysis and mechanical process according to Peng et al. [42]. Numerous methods have been established for extracting nanocellulose from cellulosic substances. These varied extraction techniques lead to differences in the types and characteristics of the nanocellulose produced. In this section, the primary methods of extraction are categorized into two types: acid hydrolysis and mechanical processing.

Cellulose underwent hydrolysis using 60% sulfuric acid at a ratio of 1:25 cellulose to sulfuric acid. This hydrolysis was performed under various concentrations of sulfuric acid, temperatures, and times. The process was halted by introducing a tenfold excess of distilled water (250 ml) into the mix. The resulting colloidal suspension was then centrifuged at 6500 rpm for 30 min. Following this, it

underwent dialysis for 5 days to neutralize to a pH range of 6–7 and remove sulfate ions. The neutral colloidal suspension was subsequently sonicated for 10 min to ensure the uniformity of the produced nanocellulose [43].

2.9 Application of anthraquinone, hydrogel, and nanocellulose

Anthraquinone, hydrogel, and nanocellulose formulations (1:1) were topically applied to the injured wound area on the backs of the rats at specific time points: days 0, 3, 6, 9, 12, 15, 17, and 19 post-wounding. The application of these treatments aimed to assess their effects on wound healing progress. Additionally, the wound area was measured during each application to monitor any changes.

2.10 Collection of tissue specimens

At the conclusion of the study, specifically 19 days post-wounding, all rats were euthanized in a humane manner through decapitation while under anesthesia, which was administered via an intraperitoneal injection of pentobarbital (500 mg/kg). The entire wound, along with a margin of approximately 5 mm of the surrounding healthy tissue, was excised. These tissue samples were then fixed in a 10% buffered formalin solution (pH 7.4) for a duration of 48 h. Following fixation, the samples were embedded in paraffin and prepared for subsequent histopathological and immunohistochemical (IHC) analyses.

After sample collection and termination of the study, all sacrificed rats, along with any remaining tissue samples as well as all bedding materials, were handled in accordance with strict hygienic protocols and properly disposed of in a controlled burial pit to ensure proper biosecurity measures.

2.11 Histopathological examination

The skin wound tissues were fixed in 10% formalin buffered solution (pH 7.4) for a period of 48 h. Subsequently, the fixed tissues were embedded in paraffin, sectioned, and stained with hematoxylin and eosin (H&E). The histopathological assessment encompassed the evaluation of various parameters, including the extent of granulation tissue formation, necrosis, degree of epithelialization, connective tissue remodeling, and infiltration of inflammatory cells, as previously described by Tuan et al. [44].

2.12 Immunohistochemical analysis of TGF-β1 and VEGF

Immunohistochemical staining for TGF-β1 and VEGF was carried out on all tissue specimens, utilizing sections that were 4 μm thick and embedded in paraffin, following the protocol described by Saber et al. [45]. The sections underwent deparaffinization in xylene and were rehydrated through a series of ethanol dilutions.

Reda *et al. Beni-Suef Univ J Basic Appl Sci*   (2024) 13:63

Page 6 of 11

To retrieve antigens, the sections were submerged in a 0.05 M citrate buffer solution at a pH of 6.8. Endogenous peroxidase activity was blocked by incubation in a 0.3% H_2O_2 in methanol solution for 20 min at room temperature (RT). To prevent non-specific binding, the sections were treated with Protein Block Serum Free for 30 min at RT. Immunolabeling of TGF-β1 was performed on all samples using an anti-TGF-β1 rabbit polyclonal antibody (BIOCYC GmbH & Co. KG, Im Biotechnologiepark TGZ I, 14,943 Luckenwalde, Germany) at a dilution of 1:50. The sections were incubated overnight in a humidified chamber at 4 °C. Similarly, immunolabeling of VEGF was performed using an anti-VEGF rabbit polyclonal antibody (49,026; BioGenix, Netherlands) at a dilution of 1:100. The sections were incubated overnight in a humidified chamber at 4 °C. Following this, all sections were washed with phosphate-buffered saline (PBS) and then incubated with a goat anti-rabbit secondary antibody (catalog number K4003, EnVision+™ System Horseradish Peroxidase Labeled Polymer; Dako) for 30 min at room temperature. After washing with PBS, the sections were visualized using liquid DAB (3,3'-diaminobenzidine) and then washed in distilled water. Counterstaining was performed using Mayer's hematoxylin. Following counterstaining, the sections were dehydrated using an alcohol gradient, cleared with xylene, and mounted for examination under a light microscope.

2.13 Statistical analysis

Statistical differences between the various groups tested were evaluated using multiple t tests (unpaired two-tailed t test), employing the Holm-Sidak method to adjust for multiple comparisons. For statistical analysis, GraphPad Prism software version 8.00 (GraphPad Software, San Diego, California, USA) was employed.

3 Results

3.1 Mortalities

Throughout the entire duration of the study, there were no recorded mortalities among the animals.

3.2 Characterization of anthraquinones

Figure 1 shows the FTIR analysis of both anthraquinone and nanocellulose where the bands or peaks were much closed and sharp spike which had the same characteristics bands. The shift vibration of C=O was detected at 1586 cm^{-1} and 1677 cm^{-1}. The small peaks shouldered just between 3449 and 3754 cm^{-1}.

3.3 Histopathological examination

The histological examination of the control group (G1) at day 19 post-wounding revealed distinct features indicative of impaired wound healing. Reactive mildly hypertrophied endothelial blood vessels were observed, extending into the markedly hyperplastic epidermis. The epidermis exhibited a clump of basal cells, hyperkeratotic features and frequently observed spongiosis. Within the epidermis, the keratinocytes appeared shrunken with pyknotic nuclei (necrotic) or swollen and rounded with vacuolated cytoplasm (Fig. 3A, B).

Group (G2), treated with hydrogel, exhibited subepidermal edema, and collagen fiber swelling associated with mild epidermal spongiosis. Additionally, inflammatory cell infiltration was evident, along with mild congestion of endothelial blood vessels (Fig. 3C, D).

In contrast, Group (G3), treated with anthraquinone, showed a different histopathological profile. The epidermis exhibited diffuse, severe irregularly hyperplastic features, accompanied by some epidermal spongiosis. Dermal edema was present, along with a few to minimal inflammatory cells infiltration. Notably, marked hyperkeratosis was observed, while the endothelial blood vessels appeared normal (Fig. 3E, F).

Group (G4), treated with anthraquinone and nanocellulose, exhibited a distinct histological pattern. The epidermal architecture appeared normal, with marked orthokeratotic hyperkeratosis. Minimal dermal edema and few perivascular inflammatory cell aggregations were observed (Fig. 3G, H).

Group (G5), treated with nanocellulose alone, exhibited specific histopathological features. The epidermis showed moderately psoriasiform hyperplastic characteristics, with prominent rete ridges and intercellular edema. Occasional epidermal necrotic cells were observed. Within the dermis, numerous inflammatory cells were present along with mild epidermal spongiosis (Fig. 3I, J).

3.4 Immunohistochemistry (IHC)

Immunohistochemical analysis was performed to evaluate the expression of both transforming growth factor β (TGF-β) and vascular endothelial growth factor (VEGF) in the skin tissues of different treated groups.

Figure 4 shows representative IHC images of TGF-β expression. In the control (G1), intense staining of TGF-β was observed in proliferating dermal extracellular matrix (ECM), extending between subcutaneous fat (Fig. 4A). In contrast, G2 exhibited few immunostained cells in both the epidermis and dermis (Fig. 4B). Notably, positive immunostaining was observed in dermal macrophages and fibroblasts (Fig. 4C). In G3, the skin layers showed no immunostaining for TGF-β (Fig. 4D). However, numerous dermal fibroblasts exhibited positive immunostaining in Fig. 4E. In G4, there was no epidermal staining observed, but dermal immunostaining was evident. Additionally, diffuse staining was observed in dermal

Reda *et al. Beni-Suef Univ J Basic Appl Sci*   (2024) 13:63

Page 7 of 11
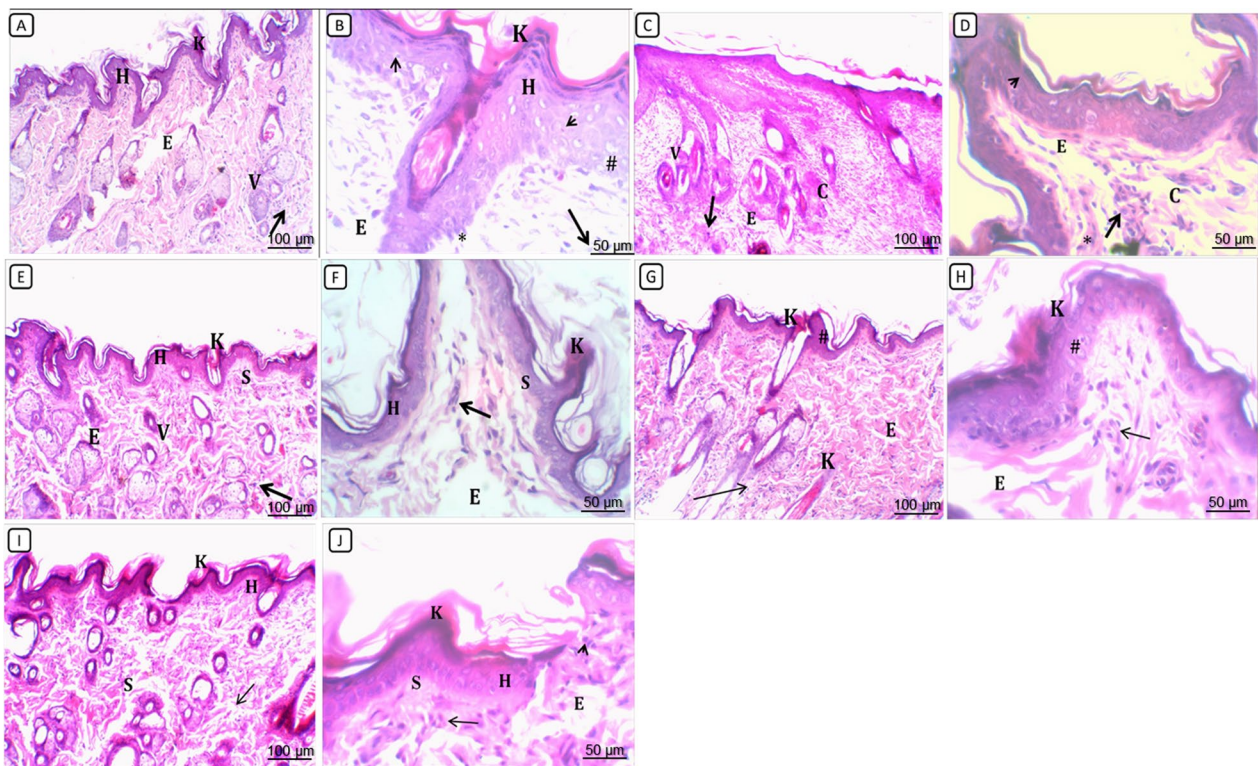
Fig. 3 Photomicrographs of skin surface: **A**, **B** control group (G1) showing expanding the dermis with edema (E) admixed with numerous eosinophils, macrophages and lymphocytes (thin arrow) around a reactive mildly hypertrophied endothelial blood vessels (V)and extending into the markedly hyperplastic (H), clump of basal cell (*) and hyperkeratotic epidermis (K), keratinocytes are shrunken and hypereosinophilic with pyknotic nuclei (necrotic) (arrow head), or are swollen and rounded with vacuolated cytoplasm (intracellular edema) (#) with H&E, (A) 100X and (B) 400X. **C**, **D** Group (G2) treated with hydrogel showing of the signs of the skin problems like epidermal liquefaction, sub-epidermal edema (E), collagen fiber swelling (C), inflammatory cell infiltration (Arrow) and mild congested endothelial blood vessels (V) with H&E, (C) 100X and (D) 400X. **E**, **F** Group (G3) treated by anthraquinone showing diffuse, severe irregularly hyperplastic epidermis (H) and diffuse epidermal spongiosis (S) with dermal edema (E) and few to minimal lymphocytic aggregations (thin arrow), marked hyperkeratosis (k) with normal endothelial blood vessels (V), with H&E, (E) 100X and (F) 400X. **G**, **H** Group (G4) treated by anthraquinone and nanocellulose showing Normally epidermal architecture (#) with marked orthokeratotic hyperkeratosis (k) and minimal dermal edema (E) and few perivascular lymphocytic aggregations (thin arrow), with H&E, (G) 100X and (H) 400X. **I**, **J** Group (G5) treated by nanocellulose showing moderately psoriasiform hyperplastic epidermis (H) with prominent rete ridges, intercellular edema (E) and occasional epidermal necrotic cells (arrow), minimal orthokeratotic hyperkeratosis (k) and within the dermis there are numerous lymphocytes, plasma cells, and eosinophil (arrow head), H&E, 100x, dermal eosinophils (thin arrow) with mild epidermal spongiosis(S) with H&E, (I) 100X and (J) 400X

fibroblasts (Fig. 4F, G). G5 showed minimal epidermal staining, while many dermal fibroblasts exhibited positive immunostaining [Fig. 4H, I].

On the other hand, Fig. 5 illustrates IHC analysis of vascular endothelial growth factor (VEGF) expression. In G1, intense staining of VEGF was observed in the dermal layer, extending toward the subcutaneous muscle (Fig. 5A). In G2, no epidermal staining was observed, but mild dermal staining for VEGF was detected (Fig. 5B). Notably, G2 exhibited intense immunostained dermal vessels, fibroblasts, and macrophages (Fig. 5C). G3 showed few immunostained areas around the hair shaft and dermis (Fig. 5D). In G4, both epidermal and dermal

immunostaining for VEGF was faint (Fig. 5E). G5 exhibited faint immunostaining in the proliferated epidermis and hair follicles (Fig. 5F).

4 Discussion

Wound healing encompasses a multitude of cellular and molecular mechanisms, making it a complicated process aimed to restore the integrity of damaged tissues [46]. This research explored the capabilities of a nanocellulose-based anthraquinone derived from marine fungi as an alternative therapy for skin wound healing in a rat model. The results demonstrated the histopathological and

Reda *et al. Beni-Suef Univ J Basic Appl Sci*   (2024) 13:63

Page 8 of 11
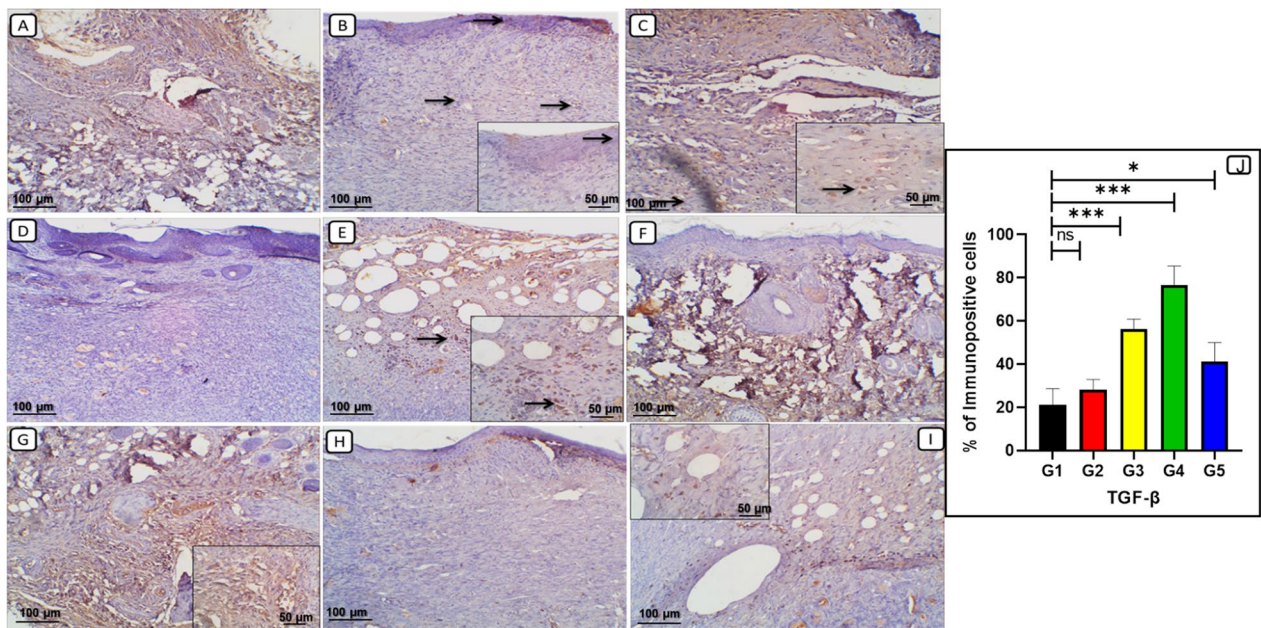
Fig. 4 Representative immunohistochemistry (IHC) of transforming growth factor β (TGF-β) expression in rat skin from different treated groups. **A** Control group (G1) intense staining in proliferating dermal ECM and extended in between subcutaneous fat. **B** G2 showing few immunostained epidermal and dermal cells (arrows). **C** G2 positive immunostained dermal macrophages and fibroblast. **D** G3 group showing skin layers without immunostaining. **E** G3 group showing numerous positive immunostained dermal fibroblast (arrow). **F**, **G** G4 group without epidermal staining in (F) and dermal immunostaining in (G), Inset, diffuse staining in dermal fibroblast, ECM. **H**, **I** G5 group showing few epidermal staining with many dermal positive immunostained fibroblast. IHC, A –I, 100X, inset box at 400x. **J** The percent of TGF-β positive cells. ***, $P < 0.001$; *, $P < 0.05$; ns = not significant on Student's *t* test
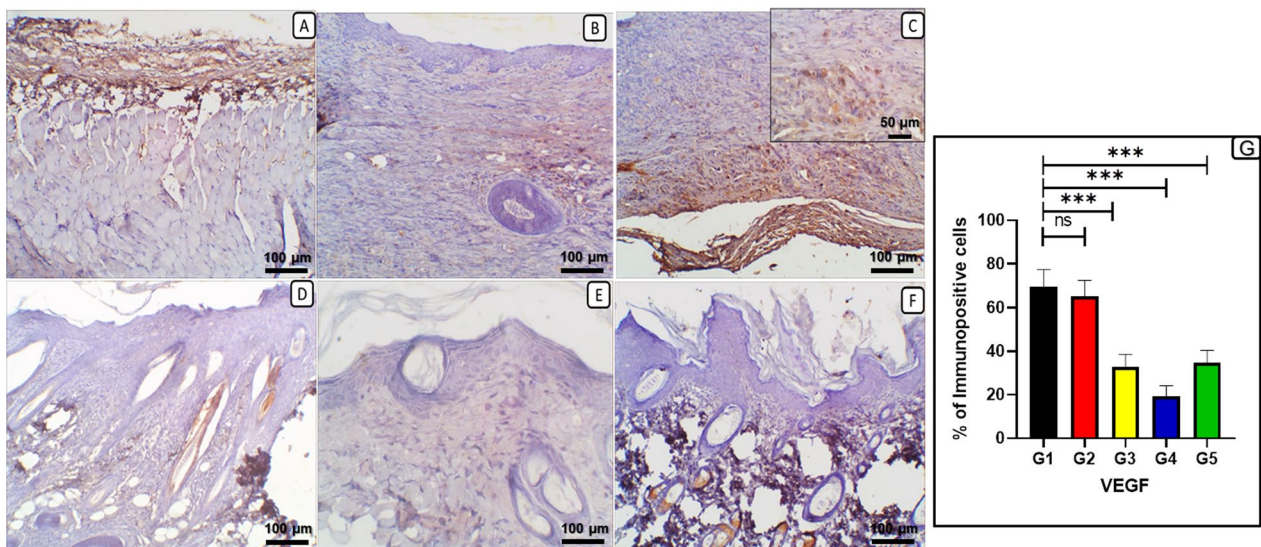
Fig. 5 Representative immunohistochemistry (IHC) of vascular endothelial growth factor (VEGF) expression in rat skin from different treated groups. **A** Control group (G1) intense staining in dermal layer that extended to subcutaneous muscle. **B** G2 showing no epidermal staining with mild dermal staining. **C** G2 showing intense immunostained dermal vessels, fibroblast and macrophages. **D** G3 group showing few immunostaining in around hair shaft and dermis. **E** G4 group showing faint epidermal and dermal immunostaining. **F** G5 group showing faint immunostaining in proliferated epidermis and in hair follicles. IHC, all pictures at 100×except figure E and the inset box at 400×**G**) The percentage of VEGF positive cells. ***, $P < 0.001$; ns = not significant on Student's *t* test

Reda *et al. Beni-Suef Univ J Basic Appl Sci*   (2024) 13:63

Page 9 of 11

immunohistochemical evidences supporting the effectiveness of this novel approach.

The choice of an appropriate wound dressing is crucial for successful wound healing. Traditional dressings have evolved over time to become interactive and bioactive solutions that promote cell regeneration, collagen synthesis, and fight against infections [47]. However, the demand for sustainable and eco-friendly materials processable at the nanoscale is on the rise. Polymers derived from biomass, like cellulose and its derivatives, have attracted considerable interest because of their inherent characteristics [48].

In this study, a nanocellulose-based wound dressing loaded with anthraquinone derived from marine fungi was utilized. The experimental animals were divided into five groups, including a control group and various treatment groups. The wound healing process was assessed by measuring the wound area at different time points. The results showed promising outcomes in terms of wound healing progression. The group treated with anthraquinone and nanocellulose demonstrated the most favorable results, with normal epidermal architecture, marked hyperkeratosis, and minimal dermal edema.

Histopathological examination of the wound tissues supported the effectiveness of the anthraquinone and nanocellulose treatment. The control group exhibited mildly hypertrophied endothelial blood vessels, hyperplastic epidermis, and shrunken or swollen keratinocytes, which are indicative of prolonged wound healing [49]. In contrast, the group treated with anthraquinone showed a significant improvement in wound healing, characterized by a severe irregularly hyperplastic epidermis and diffuse epidermal spongiosis. These findings suggest that anthraquinone treatment promotes enhanced tissue remodeling and regeneration [50].

Remarkably, the combination treatment of anthraquinone and nanocellulose resulted in the restoration of normal epidermal architecture with minimal dermal edema. This histological pattern suggests that the combination therapy enhances tissue regeneration and remodeling, which is consistent with previous studies demonstrating the beneficial effects of nanocellulose in wound healing [51]. The presence of minimal dermal edema indicates improved vascularization and efficient drainage of the wound site.

To evaluate the expression of key growth factors involved in wound healing, IHC analysis was performed, focusing on transforming growth factor β (TGF-β) and vascular endothelial growth factor (VEGF). TGF-β and VEGF play vital roles in wound healing process, especially during the early stages of healing process. TGF-β is a crucial regulator of cellular processes such as cell proliferation, extracellular matrix deposition, and tissue remodeling [52]. It promotes the differentiation of fibroblasts into myofibroblasts, which are responsible for wound contraction and collagen synthesis [53]. Additionally, TGF-β stimulates angiogenesis through induction of endothelial cells migration and proliferation [54]. VEGF, on the other hand, plays a pivotal role in angiogenesis and neovascularization, essential for providing nutrients and oxygen to the healing tissue [55]. The expression of TGF-β gradually declines during the later stages of wound healing as tissue remodeling and maturation occur, while VEGF level gradually decreases, reflecting the resolution of angiogenesis and the transition to the remodeling phase [56].

IHC staining revealed distinct patterns of TGF-β and VEGF expression among the treatment groups. In the control group, intense staining of TGF-β was observed in the proliferating dermal, suggesting its involvement in the prolonged wound healing process. In contrast, the group treated with anthraquinone showed no staining of TGF-β in epidermis, indicating a potential inhibitory effect on its expression, which is attributed to approximate epidermal growth. Importantly, the combination treatment group exhibited diffuse staining of TGF-β in dermal fibroblasts. Since TGF-β plays a crucial role in stimulating collagen synthesis and deposition by fibroblasts, promoting the formation of mature scar tissue, the combination therapy is suggested to contribute to improving wound healing outcomes [57].

Similarly, VEGF expression varied among the treatment groups. The control group showed intense staining of VEGF in the dermal layer, indicative of persistent ongoing angiogenesis during the healing process. In contrast, the group treated with anthraquinone exhibited no epidermal staining and only mild dermal staining of VEGF, suggesting a potential downregulation of VEGF expression. The combination treatment group showed faint epidermal and dermal staining of VEGF, indicating a potential modulation of VEGF expression and angiogenic processes in the wound bed.

Overall, histopathological and immunohistochemical findings provide valuable insights into the effects of anthraquinone and nanocellulose treatment on wound healing. The significant improvement in histopathological features, such as epidermal hyperplasia and spongiosis, as well as the modulation of TGF-β and VEGF expression, suggest the potential of this combination therapy in promoting tissue regeneration and angiogenesis. Further research is needed to clarify and explain the underlying mechanisms and optimize the dosage and application strategies for this promising therapeutic approach.

In **conclusion**, this research emphasizes the capabilities of a nanocellulose-based anthraquinone derived from marine fungi as a promising approach for enhancing skin

Reda *et al. Beni-Suef Univ J Basic Appl Sci*   (2024) 13:63

Page 10 of 11

wound healing. The observed histopathological improvements and modulation of TGF-β and VEGF expression support the efficacy of this novel therapy. Future studies should aim at improving the formulation and investigating its therapeutic efficacy in larger animal models, ultimately progressing to clinical trials.

Abbreviations

HPLC   High-performance liquid chromatography
FTIR   Fourier transform infrared
NMR   Nuclear magnetic resonance (NMR) spectroscopy
IHC   Immunohistochemical analyses

Availability data and materials
 All data generated or analyzed during this study are included in this published article (tables and figures and/or its Supplementary Information file).

Declarations

Ethical approval and Consent to participate
Following the normal operating procedures approved by the Institutional Animal Care and Animal Ethics Committee, Faculty Aquatic and Fisheries Sciences, Kafrelsheikh University, Egypt (IAACUC-KSU), this experiment was performed on albino rats.No human participants in the current study.

Consent for publication
Not applicable.

Competing interests
We declare there is no conflict of interest.

Author details
[1]Fish Processing and Biotechnology Department, Faculty of Aquatic and Fisheries Sciences, Kafrelsheikh University, Kafrelsheikh 33516, Egypt. [2]Clinical Pathology Department, Faculty of Veterinary Medicine, Kafrelsheikh University, Kafrelsheikh 33516, Egypt. [3]Department of Surgery, Anesthesiology and Radiology, Faculty of Veterinary Medicine, Kafrelsheikh University, Kafrelsheikh 33516, Egypt. [4]Department of Pathology, Faculty of Veterinary Medicine, Kafrelsheikh University, Kafrelsheikh 33516, Egypt. [5]Biology Department, College of Science and Humanities-Al Quwaiiyah, Shaqra University, 19257 Al Quwaiiyah, Saudi Arabia.

References

1. Wang X et al (2013) The mouse excisional wound splinting model, including applications for stem cell transplantation. Nat Protoc 8(2):302–309
2. Tyavambiza C, Meyer M, Meyer S (2022) Cellular and molecular events of wound healing and the potential of silver based nanoformulations as wound healing agents. Bioengineering 9:712
3. Liu T, Lu Y, Zhan R, Qian W, Luo G (2023) Nanomaterials and nanomaterials-based drug delivery to promote cutaneous wound healing. Adv Drug Deliv Rev 193:114670. https://doi.org/10.1016/j.addr.2022.114670
4. Napagoda M, Madhushanthi P, Witharana S (2022) Nanomaterials for wound healing and tissue regeneration. Nanotechnol Modern Med. https://doi.org/10.1007/978-981-19-8050-3_5
5. Ambekar RS, Kandasubramanian B (2019) Advancements in nanofibers for wound dressing: a review. Eur Polym J 117:304–336
6. Felgueiras HP, Tavares T, Amorim M (2019) Biodegradable, spun nanocomposite polymeric fibrous dressings loaded with bioactive biomolecules for an effective wound healing: a review. In: IOP conference series: materials science and engineering. IOP Publishing
7. Ghomi RE et al (2019) Wound dressings: current advances and future directions. J Appl Polym Sci 136(27):47738
8. Dart A, Bhave M, Kingshott P (2019) Antimicrobial peptide-based electrospun fibers for wound healing applications. Macromol Biosci 19(9):1800488
9. Chen J, Xu J, Wang K, Cao X, Sun R (2016) Cellulose acetate fibers prepared from different raw materials with rapid synthesis method. Carbohydr Polym 137:685–692
10. Golizadeh M, Karimi A, Gandomi-ravandi S, Vossoughi M, Khafaji M, Joghataei M, Faghihi F (2019) Evaluation of cellular attachment and proliferation on different surface charged functional cellulose electrospun nanofibers. Carbohydr Polym 207:796–805
11. Xu Z, Dong M, Yin S, Dong J, Zhang M, Tian R, Min W, Zeng L, Qiao H, Chen J (2023) Why traditional herbal medicine promotes wound healing: research from immune response, wound microbiome to controlled delivery. Adv Drug Deliv Rev 195:114764. https://doi.org/10.1016/j.addr.2023.114764
12. Pakpahan FD, Rahmiyani I, Sukmawan YP (2023) Wound healing activity of the clitoria ternatea L. flower ethanolic extract gel preparation in diabetic animal model. Res J Pharm Technol 16:140–144. https://doi.org/10.52711/0974-360X.2023.00026
13. Sharma R, Sharma KS, Kumar D (2022) Introduction to nanotechnology. In: Nanomaterials in clinical therapeutics: synthesis and applications. https://doi.org/10.1002/9781119857747.ch1
14. Baig N, Kammakakam I, Falath W (2021) Nanomaterials: a review of synthesis methods, properties, recent progress, and challenges. Mater Adv 2(6):1821–1871. https://doi.org/10.1039/d0ma00807a
15. Bhardwaj N, Chouhan D, Mandal BB (2017) Tissue engineered skin and wound healing: current strategies and future directions. Curr pharmaceut Des 23(24):3455–3482. https://doi.org/10.2174/138161282366617052609 4606
16. Wang W, Lu KJ, Yu CH, Huang QL, Du YZ (2019) Nano-drug delivery systems in wound treatment and skin regeneration. J Nanobiotechnol 17(1):82. https://doi.org/10.1186/s12951-019-0514-y
17. Bugni TS, Ireland CM (2004) Marine-derived fungi: a chemically and biologically diverse group of microorganisms. Nat Prod Rep 21(1):143–163
18. Krychowiak M, Grinholc M, Banasiuk R, Krauze-Baranowska M, Głód D, Kawiak A, Królicka A (2014) Combination of silver nanoparticles and Drosera binata extract as a possible alternative for antibiotic treatment of burn wound infections caused by resistant Staphylococcus aureus. PLoS ONE 9(12):e115727. https://doi.org/10.1371/journal.pone.0115727. (**PMID:25551660;PMCID:PMC4281117**)
19. Greco G, Turrini E, Catanzaro E, Fimognari C (2021) Marine anthraquinones: pharmacological and toxicological issues. Mar Drugs 19(5):272. https://doi.org/10.3390/md19050272
20. Sebak M, Molham F, Greco C, Tammam MA, Sobeh M, El-Demerdash A (2022) Chemical diversity, medicinal potentialities, biosynthesis, and pharmacokinetics of anthraquinones and their congeners derived from marine fungi: a comprehensive update. RSC Adv 12:24887–24921
21. Hafez Ghoran S, Taktaz F, Ayatollahi SA, Kijjoa A (2022) Anthraquinones and their analogues from marine-derived fungi: chemistry and biological activities. Mar Drugs 20:474
22. Fouillaud M, Venkatachalam M, Girard-Valenciennes E, Caro Y, Dufossé L (2016) Anthraquinones and derivatives from marinederived fungi: structural diversity and selected biological activities. Mar Drugs 14:64
23. Malik EM, Müller CE (2016) Anthraquinones as pharmacological tools and drugs. Med Res Rev 36:705–748. https://doi.org/10.1002/med.21391

24. Wuthi-udomlert M, Kupittayanant P, Gritsanapan W (2018) In vitro evaluation of antifungal activity of anthraquinone derivatives of Senna alata. J Health Res 24:117–122

25. Preet G, Gomez-Banderas J, Ebel R, Jaspars M (2022) A structure-activity relationship analysis of anthraquinones with antifouling activity against marine biofilm-forming bacteria. Front Nat Produc 1:990822. https://doi.org/10.3389/fntpr.2022.990822

26. Osman CP, Ismail NH (2018) Antiplasmodial anthraquinones from medicinal plants: The chemistry and possible mode of actions. Nat Prod Commun 13:1934578X1801301. https://doi.org/10.1177/1934578X1801301207

27. Chien S-C, Wu Y-C, Chen Z-W, Yang W-C (2015) Naturally occurring anthraquinones: chemistry and therapeutic potential in autoimmune diabetes. Evid-Based Compl Alt 2015:1–13

28. Kshirsagar AD, Panchal PV, Harle UN, Nanda RK, Shaikh HM (2014) Anti-inflammatory and antiarthritic activity of anthraquinone derivatives in rodents. Int J Inflam 2014:690596. https://doi.org/10.1155/2014/69059

29. Wu C-M, Wu S-C, Chung W-J, Lin H-C, Chen K-T, Chen Y-C et al (2007) Antiplatelet effect and selective binding to cyclooxygenase (COX) by molecular docking analysis of flavonoids and lignans. Int J Mol Sci 8:830–841. https://doi.org/10.3390/i8080830

30. Seo EJ, Ngoc TM, Lee S-M, Kim YS, Jung Y-S (2012) Chrysophanol-8-O-glucoside, an anthraquinone derivative in rhubarb, has antiplatelet and anticoagulant activities. J Pharmacol Sci 118:245–254

31. Jackson TC, Verrier JD, Kochanek PM (2013) Anthraquinone-2-sulfonic acid (AQ2S) is a novel neurotherapeutic agent. Cell Death Dis 4:e451

32. Malik EM, Müller CE (2016) Anthraquinones as pharmacological tools and drugs. Med Res Rev 36:705–748

33. Tian W, Wang C, Li D, Hou H (2020) Novel anthraquinone compounds as anticancer agents and their potential mechanism. Fut Med Chem 12(7):627–644

34. Srinivas G, Babykutty S, Sathiadevan PP, Srinivas P (2007) Molecular mechanism of emodin action: transition from laxative ingredient to an antitumor agent. Med Res Rev 27:591–608. https://doi.org/10.1002/med.20095

35. Huang Q, Lu G, Shen H-M, Chung MCM, Ong CN (2007) Anti-cancer properties of anthraquinones from rhubarb. Med Res Rev 27:609–630

36. Atiba A et al (2011) Aloe vera oral administration accelerates acute radiation-delayed wound healing by stimulating transforming growth factor-β and fibroblast growth factor production. Am J Surg 201(6):809–818

37. Oliveira DGP, Pauli G, Mascarin GM, Delalibera I (2015) A protocol for determination of conidial viability of the fungal entomopathogens Beauveria bassiana and Metarhizium anisopliae from commercial products. J Microbiol Methods 119:44–52

38. Toma MA, Nazir KNH, Mahmud MM, Mishra P, Ali MK, Kabir A, Shahid MAH, Siddique MP, Alim MA (2021) Isolation and identification of natural colorant producing soil-borne Aspergillus niger from Bangladesh and extraction of the pigment. Foods 10(6):1280

39. Zhang H, Bai X, Wu B (2012) Evaluation of antimicrobial activities of extracts of endophytic fungi from Artemisia annua. Bangladesh J Pharmacol 7(2):120–123

40. Harborne AJ (1998) Phytochemical methods a guide to modern techniques of plant analysis. Springer Science & Business Media

41. Riaz T, Zeeshan R, Zarif F, Ilyas K, Muhammad N, Safi SZ, Rahim A, Rizvi SA, Rehman IU (2018) FTIR analysis of natural and synthetic collagen. Appl Spectrosc Rev 53(9):703–746

42. Peng BL, Dhar N, Liu HL, Tam KC (2011) Chemistry and applications of nanocrystalline cellulose and its derivatives: a nanotechnology perspective. Can J Chem Eng 89(5):1191–1206

43. Wang XH, Wu SY, Zhen YS (2004) Inhibitory effects of emodin on angiogenesis. Yao Xue Xue Bao 39(4):254–258

44. Tuan RS, Baksh D, Song L (2004) Adult mesenchymal stem cells: characterization, differentiation, and application in cell and gene therapy. J Cell Mol Med 8(3):301–316

45. Saber S et al (2019) Olmesartan ameliorates chemically-induced ulcerative colitis in rats via modulating NFκB and Nrf-2/HO-1 signaling crosstalk. Toxicol Appl Pharmacol 364:120–132

46. Sen CK et al (2009) Human skin wounds: a major and snowballing threat to public health and the economy. Wound Repair Regen 17(6):763–771

47. Gurtner GC et al (2008) Wound repair and regeneration. Nature 453(7193):314–321

48. Seddiqi H et al (2021) Cellulose and its derivatives: towards biomedical applications. Cellulose 28(4):1893–1931

49. Gushiken LFS et al (2021) Cutaneous wound healing: an update from physiopathology to current therapies. Life 11(7):665

50. Farci F, Mahabal GD (2023) Hyperkeratosis. In: StatPearls [Internet]. Treasure Island (FL): StatPearls Publishing. PMID: 32965877

51. Resch A, Staud C, Radtke C (2021) Nanocellulose-based wound dressing for conservative wound management in children with second-degree burns. Int Wound J 18(4):478–486

52. Bonnans C, Chou J, Werb Z (2014) Remodelling the extracellular matrix in development and disease. Nat Rev Mol Cell Biol 15(12):786–801

53. Kahata K, Dadras MS, Moustakas A (2018) TGF-β family signaling in epithelial differentiation and epithelial-mesenchymal transition. Cold Spring Harb Perspect Biol 10(1):a022194

54. Ferrari G et al (2012) TGF-β1 induces endothelial cell apoptosis by shifting VEGF activation of p38(MAPK) from the prosurvival p38β to proapoptotic p38α. Mol Cancer Res 10(5):605–614

55. Shibuya M (2011) Vascular endothelial growth factor (VEGF) and its receptor (VEGFR) signaling in angiogenesis: a crucial target for anti- and pro-angiogenic therapies. Genes Cancer 2(12):1097–1105

56. Penn JW, Grobbelaar AO, Rolfe KJ (2012) The role of the TGF-β family in wound healing, burns and scarring: a review. Int J Burns Trauma 2(1):18–28

57. Savari R et al (2019) Expression of VEGF and TGF-β genes in skin wound healing process induced using phenytoin in male rats. Jundishapur J Health Sci 11(1):1

Publisher's Note

Springer Nature remains neutral with regard to jurisdictional claims in published maps and institutional affiliations.